Modelling and upscaling analysis of gas diffusion electrode based electrochemical carbon dioxide reduction systems

Ziming Yang[a], Da Li[b,c], Lei Xing[a], Hang Xiang[b], Jin Xuan[c], Shaoan Cheng[d], Eileen Hao Yu[b, c*], Aidong Yang[a*]

[a]Department of Engineering Science, University of Oxford, Parks Road, Oxford, OX1 3PJ, United Kingdom

[b]School of Engineering, Newcastle University, Newcastle Upon Tyne, NE1 7RU, United Kingdom

[c] Department of Chemical Engineering, Loughborough University, LE11 3TU, United Kingdom

[d] State Key Laboratory of Clean Energy Utilization, Zhejiang University, Hangzhou, China

*Corresponding authors. E-mail address:

aidong.yang@eng.ox.ac.uk;

e.yu@lboro.ac.uk

Abstract

As an emerging technology for CO_2 utilisation, electrochemical CO_2 reduction reaction (ECO2RR) systems incorporating gas diffusion electrodes (GDE) have the potential to transform CO_2 to valuable products efficiently and environment-friendly. In this work, a two-dimensional multiphase model capturing the details of the catalyst layer in a GDE that produces formate with by-products is established and quantitatively validated against experimental data. This model is capable of describing the mixture gas and aqueous species transportation, electron conduction processes and a series of interrelated chemical and electrochemical

reactions. Specific electrical energy consumption (SEEC) and product yield (PY) have been introduced and used to examine the GDE scalability and evaluate the system performance. The results predict the optimal values for applied cathode potential and catalyst loading and porosity. The effect of inlet gas composition and velocity is also evaluated. Moreover, this study predicts that the GDE is scalable as it retains a stable performance as its geometrical surface area varies. This model together with the simulation findings contributes to the improved understanding of GDE-based CO_2 conversion as needed for the future development towards successful industrial applications.

Keywords

Electrochemical CO_2 reduction; Gas diffusion electrode; Modelling; Scalability; Energy consumption; Yield; Optimisation

Introduction

Electrochemical CO_2 reduction reaction (ECO2RR) has recently emerged as one of the carbon capture and utilisation (CCU) technologies, which transforms CO_2 to valuable chemicals by consuming water and electricity.[1,2] Depending on the catalyst type, CO_2 can be reduced to different products such as syngas, methane (CH_4), formate ($HCOO^-$) and ethyl alcohol (C_2H_5OH) in the cathodic compartment.[1,3] Currently, its application is significantly limited by the low current density, mainly owing to the large CO_2 mass transfer resistance and the undesirable competitive hydrogen evolution reaction (HER).[1–5] Gas diffusion electrode (GDE) offers a prospect to the improvement of the overall performance of an ECO2RR electrolyser under mild operating conditions (i.e. room temperature and ambient pressure).[1,4]

Different from the most frequently adopted conventional two-chamber electrolyser, where CO_2 is purged into the cathode chamber[4] or supplied via the CO_2-saturated catholyte[3], the reactant gaseous CO_2 is directly fed

into the gas chamber (GASC) and diffused through the gas diffusion layer (GDL) into the catalyst layer (CL). Compared to the planar electrode, the CL remarkably enlarges the specific area for ECO2RR reaction, alleviates the mass transfer constraint of dissolved CO_2 and reduces the ohmic loss by shortening the distance of reactant to the reaction sites and avoiding bubble appearance.[1–3,6–9] Readers can refer to the literature that systematically reviewed the fundamental knowledge and development of GDE for more details.[1] Despite of the moderate-to-high current densities achieved,[10] there is much room for GDEs to become more competitive than their traditional counterparts (i.e. electrolyser for water splitting), eventually accomplishing successful.[1,2,11]

To date, most research on ECO2RR is dedicated to experimentally developing stable, efficient and selective catalysts.[2] Limited attention has been paid to the optimisation of electrode configuration and operational conditions,[9,12] and even fewer studies focus on upscaling.[8,11,13–15] In addition to the experimental studies, model-based analysis is instrumental to promote the transition from bench-scale research to industrial-scale applications. The first GDE model for the CO_2 reduction process, a two-dimensional model of the cathode GDE in a continuous CO_2 electrolyser for formate production, was constructed on the basis of Li & Oloman cathodic model[13] by introducing fluid dynamics and more sophisticated electrochemical kinetics.[16] Subsequently, a full-cell model comprising both anode and cathode GDEs for converting CO_2 to CO[17] was proposed. These studies treated the whole GDE as a single porous medium and assumed that gaseous CO_2 was able to be adsorbed onto the catalyst and react with the electrolyte directly, yet to reflect the experimental findings that only dissolved $CO_2(aq)$ is the active reactant for electrochemical reactions.[4] In 2016, a full-cell model for electrochemical conversion of CO_2 to formate was developed to integrate the multiphase flow in the catholyte, the CO_2 adsorption process and transportation through membrane, which was then used in a scale-up analysis to assess the impact of cell height.[18] Recently, a GDE model accounting for the local details of the CL was developed.[3] Further work extended the model to include the anode and an investigation of the temperature and water variation for the membrane-electrode-assemblies (MEAs).[19,20] However, restricted by the one-dimensional (1D)

nature, the gas chamber in these studies was assumed isotropic, which ignored the spatial variation along the direction of the feed gas flow and, as recognised in previous work,[3] may introduce inaccuracy in the predicted current density distribution. Moreover, these proposed multiphysics models[3,19,20] generally require further experimental validation. These deficiencies would restrict the application of mathematical modelling in systematically supporting the future development (including up-scaling) of GDE-based ECO2RR system.

In this paper, a two-dimensional steady-state multiphase GDE model describing inter- and intra-phase mass transfer, electrochemical kinetics and aqueous-phase reactions is reported. The modelled system converts CO_2 to CO and formate with the latter selected as our target product due to its industrial importance and commercial potential.[5] Here, we present an experimental validation of our model, and subsequently use the model for predicting the scalability of the GDE and the influence of several key parameters on the system's performance. To the best of our knowledge, this is the first report of a GDE model for multiple CO_2-reduction products with a detailed account of reaction kinetics and mass transfer and applied to investigate the GDE scalability and selectivity, which are both important for the industrial application of this technology.

Model development and model-based evaluation

Description of the GDE

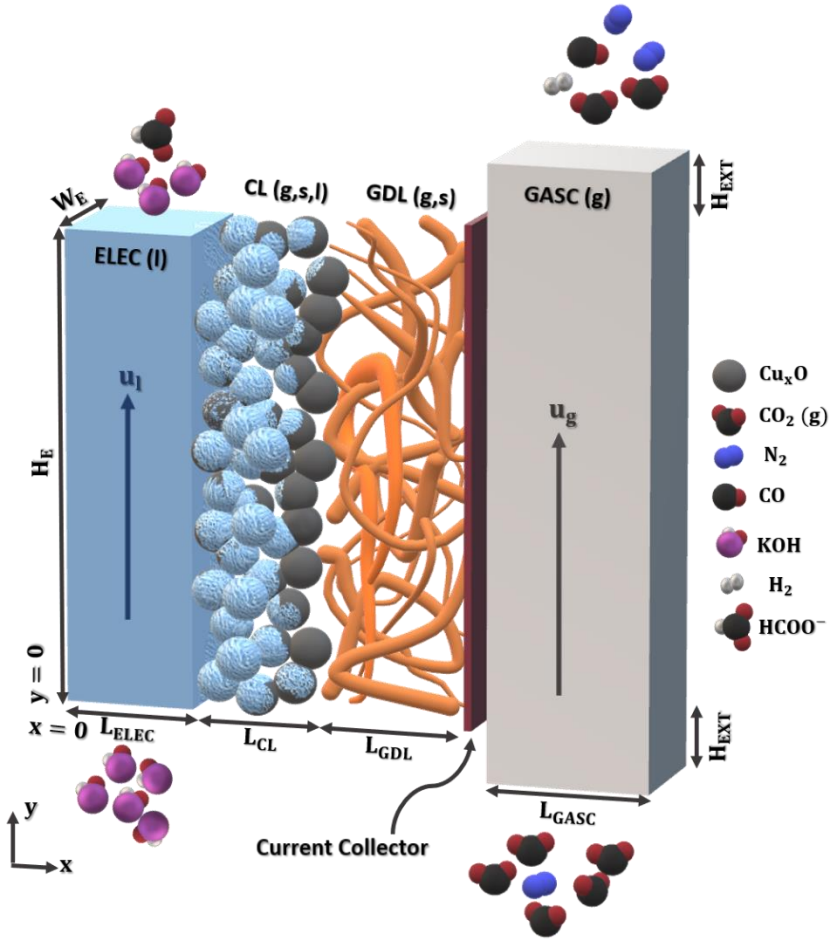

Figure 1 Schematic GDE model.

As shown in Figure 1, our GDE model comprises, from left to right, electrolyte channel (ELEC), CL, GDL and GASC. They are parallel rectangular compartments with identical heights (y-axis) and widths but different thicknesses (x-axis). The feed gas is supplied into the system from the bottom of the GASC and escapes together with other gaseous products (i.e. CO, H_2) at the other side. The current collector[4] between the GASC and the GDL, with negligible ohmic loss compared to the GDL and the CL, serves the purpose of providing electrons. CO_2 and electrons are transported via diffusion and conduction respectively through the porous hydrophobic GDL and react in the CL. The GDL in our case is a single-layer GDL.[21] As mentioned earlier, it is widely accepted that the

dissolved $CO_2(aq)$ is the only active reactant for electrochemical reactions, rather than HCO_3^-, CO_3^{2-} or $CO_2(g)$.[22–26] Thus, the gas-liquid mass transfer for CO_2 and homogeneous (aqueous-phase) reactions which consume $CO_2(aq)$ in the CL should be considered. The CL is a layer coated with the granular catalyst of Cu_xO (a mixture of Cu_2O, CuO and Cu), a non-toxic and abundant choice attractive for upscaling and also with a promise for the generation of multi-carbon products.[4,27,28] The electrolyte (potassium hydroxide, KOH) and the aqueous products (i.e. formate) flow through the ELEC. In our case, two competing CO_2 electrochemical reduction reactions occur in the CL:

$$CO_2(aq) + H_2O + 2e^- \leftrightarrow HCOO^- + OH^- \quad \text{(Ea)}$$

$$CO_2(aq) + H_2O + 2e^- \leftrightarrow CO + 2OH^- \quad \text{(Eb)}$$

In addition to CO_2 reduction reactions, as mentioned earlier, an unwanted parasitic HER also takes place in the CL simultaneously. The HER in the alkaline condition is represented as:

$$2H_2O + 2e^- \leftrightarrow H_2 + 2OH^- \quad \text{(Ec)}$$

The established two-dimensional, steady state model simulates a multiphase GDE which is assumed isothermal since the level of current density[17,29] means moderate generation of heat which on the other hand is continuously carried away by the electrolyte flow.[17,29] The x- and y- dimensions of the model are illustrated in Figure 1. The geometric parameters, which follow the experimental study,[4] are tabulated in the SI Table S2.

Gaseous species

Gaseous species (i.e. $CO_2(g)$, N_2, H_2 and CO) are considered in the GASC, the GDL and the CL; their mass conservation is modelled by Eq. (1). The mixture-averaged diffusion model is employed here to evaluate

multicomponent diffusive fluxes without an excessive computational cost.[3,19,20,30,31] The Soret effect is not considered in the diffusion term due to the isothermal assumption.[32]

$$\nabla \cdot \left(-\rho_g D_{i,m} \nabla \omega_i - \rho_g \omega_i D_{i,m} \frac{\nabla M_g}{M_g} \right) + \nabla \cdot (\rho_g u_g \omega_i) = R_{i,m} \quad (1)$$

where i denotes the gaseous species; ρ_g represents the mixture gas density; ω_i denotes the mass fraction of gaseous species; M_g is the averaged molar weight of mixture gas, which is calculated by $(\sum_i \frac{\omega_i}{M_i})^{-1}$; M_i is the molar weight of gaseous species; $D_{i,m}$ is the diffusivity of each gaseous species in the medium, m; u_g is mixture gas velocity. The source term $R_{i,m}$ for each species in the GASC and the GDL is zero; in the CL it can be found in the SI Table S1.

The gaseous diffusivity, $D_{i,m}$ is derived from the Maxwell-Stefan equation and simplified by assuming all other gaseous species have same velocities:

$$D_{i,m} = \frac{1 - \omega_i}{\sum_{k \neq i} \frac{x_k}{D_{ik}}} \quad (2)$$

where D_{ik} is the binary diffusivities for the species pairs present; x_k denotes the molar fraction of gaseous species, k. In comparison with other mixture gas models such as Maxwell-Stefan, this assumption makes $D_{i,m}$ to be determined by those parameters that are easily obtained.[30–32]

The gas velocity, u_g is solved by momentum balance together with overall mass balance. It is assumed that the gas mixture flow in the open channel of the GASC is laminar and compressible ($Ma < 0.3$).[17]

$$\rho_g (u_g \cdot \nabla) u_g = \nabla \cdot \left[-PI + \mu_g \left(\nabla u_g + (\nabla u_g)^T \right) - \frac{2}{3} \mu_g (\nabla \cdot u_g) I \right] + \rho_g g \quad (3)$$

$$\nabla \cdot (\rho_g u_g) = 0 \tag{4}$$

where P is the total gas pressure; μ_g is dynamic viscosity of the gas mixture; I is the identity tensor and g is the gravitational acceleration.

In porous media of the GDL and the CL, $D_{i,m}$ in Eq. (1) is corrected for the effective porosity for gas, $\epsilon_{m,g}^{eff}$ by using the Bruggeman equation:[3]

$$D_{i,m}^{eff} = \frac{1 - \omega_i}{\sum_{k \neq i} \frac{x_k}{(\epsilon_{m,g}^{eff})^{1.5} D_{ik}}} \tag{5}$$

It is generally assumed that electrochemical reactions can only occur at the active sites in the CL, where the electrolyte, the reactant and the catalyst meet, also regarding as three-phase interface.[3,16,17] This requires the pores in the CL to be partially or completely wetted. We define S_m as the saturation coefficient, representing the ratio of liquid occupied volume to the total volume of the pores in the medium, m. It is assumed that the factors affecting saturation (e.g. pore hydrophobicity and size distribution, capillary pressure, etc.[3,33]) remain unchanged and therefore the saturation coefficient is constant. The value of 0.5 is applied for the saturation coefficient in the CL, S_{CL} in our case (the detailed calculation method can be found in the SI section III). Same to the treatment in the prior modelling work,[3] GDL is assumed as completely dry (I.e. $S_{GDL} = 0$). The relationship between $\epsilon_{m,g}^{eff}$ and S_m is:

$$\epsilon_{m,g}^{eff} = \epsilon_m^0 (1 - S_m) \tag{6}$$

where ϵ_m^0 represents the intrinsic porosity in the medium, m, which is defined as the ratio of the total volume occupied by the pores and the total volume of the medium and assumed as constant and isotropic. ϵ_{CL}^0 is calculated by:

$$\epsilon_{CL}^{0} = 1 - \frac{m_{cat}}{\rho_{cat} L_{CL}} \quad (7)$$

where m_{cat} is the mass loading of catalyst (mass of catalyst per geometrical electrode surface area); ρ_{cat} denotes the catalyst density. Neglecting any effect of bubbles, the pores in the CL are assumed to be occupied by a static liquid phase and the gas mixture with the effective porosity, $\epsilon_{m,g}^{eff}$.[3,16] Momentum balance for laminar flow in the porous media becomes Darcy's law, in order to model mixture gas transport.[3,19,20,34]

$$u_g = -\frac{\kappa_{m,g}^{eff}}{\mu_g}(\nabla P + \rho_g g) \quad (8)$$

where $\kappa_{m,g}^{eff}$ is the effective permeability for gas in the porous medium, m. Its value for a Darcian flow in the CL, which is assumed to be occupied by uniform spherical shape catalysts with a mono-disperse size distribution, is estimated by the Kozeny-Carman equation:[35,36]

$$\kappa_{CL,g}^{eff} = \frac{d_{cat}^2}{180} \frac{(\epsilon_{CL,g}^{eff})^3}{(1 - \epsilon_{CL,g}^{eff})^2} \quad (9)$$

where d_{cat} is the diameter of catalyst particles. The effective permeability for the fibrous media, the GDL depends strongly on the intrinsic porosity and is given by: [3,36–38]

$$\kappa_{GDL,g}^{eff} = \frac{\kappa_{GDL}^{0} {\epsilon_{GDL}^{0}}^3}{(1 - \epsilon_{GDL}^{0})^2}(1 - S_{GDL})^3 \quad (10)$$

It is worth noting that the GDL may face the 'flooding' problem (i.e. electrolyte penetrates through the CL and goes into GDL) and become wetted in reality.[1,12] In this case, the effective gaseous diffusivity (see Eqs. (5) and (6)) and permeability (see Eq. (10)) would decrease, potentially leading to poor GDE performance. Incorporating this detail would require modifications to the affected equations in the future.

The overall mass balance in the GDL and the CL is analogous to that of the GASC:

$$\nabla \cdot (\rho_g u_g) = Q_m \tag{11}$$

where Q_m is the source term, which is zero for the GDL and the sum of gaseous reaction rates in the CL (see SI Table S1).

N_2 mass fraction is determined by following mass constraint:

$$\sum \omega_i = 1 \tag{12}$$

Aqueous species

The mass conservation of aqueous species, j is modelled by the Nernst-Plank equation Eq. (13):

$$\nabla \cdot \left(-\rho_l D_{j,m} \nabla \omega_j - \frac{z_j F \rho_l \omega_j D_{j,m} \nabla V_l}{R_{ideal} T} + \rho_l \omega_j u_l \right) = R_{j,m} \tag{13}$$

where ρ_l is the density of the liquid mixture; z_j is the valence of ionic species; R_{ideal} is the ideal gas constant; T is operating temperature; u_l is the liquid velocity, which is the ratio of volumetric flowrate to cross section area of the ELEC, q_l/A_{ELEC}; $D_{j,m}$ is the diffusivity of aqueous species and it is also corrected by the Bruggeman relationship in the porous medium, m.[39] The term of $R_{j,m}$ in CL is listed in the SI Table S1.

Homogenous reactions

With fresh KOH as the electrolyte being continuously supplied and the CL being sufficiently thin,[4] it is assumed that the pH (and hence the concentration of OH^-, C_{OH}) in both the ELEC and the liquid phase in the CL maintain constant at the same value as feed concentration. Hereby we only consider homogeneous reactions under the alkaline condition:

$$CO_2(aq) + OH^- \xrightarrow{k_{Ha}} HCO_3^- \quad \text{(Ha)}$$

$$HCO_3^- + OH^- \xrightarrow{k_{Hb}} H_2O + CO_3^{2-} \quad \text{(Hb)}$$

Reaction rates for Ha and Hb are expressed as:

$$R_{Ha} = k_{Ha} C_{CO_2(aq)} C_{OH} - \frac{k_{Ha}}{K_{Ha}} C_{HCO_3} \quad (14)$$

$$R_{Hb} = k_{Hb} C_{HCO_3} C_{OH} - \frac{k_{Hb}}{K_{Hb}} C_{CO_3} \quad (15)$$

where k_{Ha}, k_{Hb} are the forward reaction constants; K_{Ha}, K_{Hb} are the equilibrium constants for the reaction Ha and Hb, respectively. It is worthy to note here that, for the partially wetted porous CL, the reaction rate, R_{Ha} and R_{Hb} should be scaled by the $S_{CL}\epsilon_{CL}^0$, according to the volume averaged model.[40]

Homogenous reaction rates for $CO_2(aq)$, HCO_3^- and CO_3^{2-} are:

$$R_{H,CO_2(aq)} = -M_{CO_2} R_{Ha};\ R_{H,HCO_3} = M_{HCO_3}(R_{Ha} - R_{Hb});\ R_{H,CO_3} = M_{CO_3} R_{Hb}; \quad (16)$$

where M_{CO_2}, M_{HCO_3} and M_{CO_3} are molecular weight for CO_2, HCO_3^- and CO_3^{2-}, respectively.

Gas-liquid mass transfer

For the gas-liquid mass transfer in the CL, we only consider it for CO_2 due to the negligible solubility of CO and H_2.[19] Given the operating temperature,[4] water condensation/evaporation is also ignored. The gas-liquid mass transfer rate for CO_2 is written as:

$$R_{P,CO_2(aq)} = -R_{P,CO_2(g)} = a_{gl} K_{GL} M_{CO_2} \left(\frac{P_{CO_2(g)}}{H_{CO_2}} - C_{CO_2(aq)}\right) \quad (17)$$

where a_{gl} is the specific gas-liquid interfacial area; K_{GL} is the overall mass transfer coefficient; H_{CO_2} is Henry's constant for CO_2 and has been calculated taking into account the salting-out effect (see SI section VII); $P_{CO_2(g)}$ is the partial pressure of $CO_2(g)$, which is calculated according to Dalton's law: $P_{CO_2(g)} = P_{CL}x_{CO_2(g)}$; $C_{CO_2(aq)}$ is the concentration of dissolved CO_2 in the electrolyte. a_{gl} is given by (see SI section III):

$$a_{gl} = 2\frac{\epsilon_{CL}^{0}(r_{p,CL} - \delta_{ele})}{{r_{p,CL}}^{2}} \tag{18}$$

Electrode kinetics

With the understanding that the rate-determining step (RDS) for each of reactions (Ea) to (Ec) is that of one-electron transfer,[41,42] the current densities corresponding to the reactions (Ea) to (Ec), i_{Ea}, i_{Eb} and i_{Ec} are obtained according to the Tafel kinetics:[38]

$$i_{Ea} = -i_{o,Ea}^{ref}\left(\frac{C_{CO_2(aq)}}{C_{CO_2(aq),Ea}^{ref}}\right)\exp\left(-\frac{\beta_{Ea}F}{R_{ideal}T}\left(V_s - V_l - V_{eq,Ea}^{ref}\right)\right) \tag{19}$$

$$i_{Eb} = -i_{o,Eb}^{ref}\left(\frac{C_{CO_2(aq)}}{C_{CO_2(aq),Eb}^{ref}}\right)\exp\left(-\frac{\beta_{Eb}F}{R_{ideal}T}\left(V_s - V_l - V_{eq,Eb}^{ref}\right)\right) \tag{20}$$

$$i_{Ec} = -i_{o,Ec}^{ref}\exp\left(-\frac{\beta_{Ec}F}{R_{ideal}T}\left(V_s - V_l - V_{eq,Ec}^{ref}\right)\right) \tag{21}$$

where $i_{o,Ea}^{ref}$ $i_{o,Eb}^{ref}$ and $i_{o,Ec}^{ref}$ are the exchange current densities per catalyst surface area at the reference condition; $C_{CO_2(aq),Ea}^{ref}$, $C_{CO_{2(aq)},Eb}^{ref}$ are the reference concentrations of $CO_2(aq)$ corresponding to reaction (Ea) and (Eb), respectively; β_{Ea}, β_{Eb} and β_{Ec} denote the symmetry factor corresponding to the formation of $HCOO^-$, CO and H_2, respectively; F is the Faraday constant; $V_{eq,Ea}^{ref}$, $V_{eq,Eb}^{ref}$ and $V_{eq,Ec}^{ref}$ are the equilibrium potentials for the reactions (Ea) to (Ec) in the reference condition and the operating temperature, respectively.

The local electronic and electrolyte potential, V_s and V_l are derived by Ohm's law coupled with the charge conservation:[17]

$$\nabla \cdot \left(-\sigma_{s,m}^{eff} \nabla V_s\right) = Q_{s,m} \tag{22}$$

$$\nabla \cdot \left(-\sigma_{l,m}^{eff} \nabla V_l\right) = Q_{l,m} \tag{23}$$

where $\sigma_{s,m}^{eff}$ and $\sigma_{l,m}^{eff}$ are effective conductivities for solid material and electrolyte, respectively. Both of them are assumed constant and are corrected for $(1-\epsilon_m)$ and $\epsilon_m S_m$ respectively in the porous media according to the Bruggeman equation;[39,43,44] $Q_{s,m}$ and $Q_{l,m}$ are the source terms. $Q_{s,GDL}$ and $Q_{l,ELEC}$ are equal to zero due to the absence of electrochemical reactions; in the CL, they have same values but with opposite sign:[3,38]

$$-Q_{s,CL} = Q_{l,CL} = a_{sl}(i_{Ea} + i_{Eb} + i_{Ec}) \tag{24}$$

Electrochemical reaction rates for $CO_2(aq)$, $HCOO^-$, CO and H_2 are expressed based on Faraday's law:

$$\begin{gathered} R_{E,CO_2(aq)} = \frac{M_{CO_2} a_{sl}(i_{Ea}+i_{Eb})}{2F};\ R_{E,HCOO} = -\frac{M_{HCOO} a_{sl} i_{Ea}}{2F}; \\ R_{E,CO} = -\frac{M_{CO} a_{sl} i_{Eb}}{2F};\ R_{E,H_2} = -\frac{M_{H_2} a_{sl} i_{Ec}}{2F} \end{gathered} \tag{25}$$

where M_{HCOO}, M_{CO} and M_{H_2} are molecular weight for $HCOO^-$, CO and H_2, respectively.

a_{sl} is the specific solid-liquid interfacial area and expressed as follows (see SI section III):

$$a_{sl} = 2\frac{\epsilon_{CL}^0}{r_{p,CL}} \tag{26}$$

Boundary conditions

The gaseous species in the GASC, the GDL and the CL are modelled collectively. At the inlet of the GASC, the mixture gas composition and velocity are set as identical to those of the inlet mixture gas.[17] Ambient pressure (i.e.$1\mathrm{atm}$) with non-diffusive species is set for the outlet mixture gas at the outlet of the GASC. Zero-flux for gaseous species is applied at the ELEC/CL interface by assuming that any gas can only escape from the GASC. The pressure is continuous at the GDL/GASC interface.

For the aqueous species, we model them in the CL and the ELEC collectively. Mass fractions at the ELEC inlet (i.e. $\mathrm{y} = 0$) are set according to those of the electrolyte feed. The aqueous mass flux at the CL/GDL interface is set to zero assuming no electrolyte leakage.

For the electronic potential, constant applied cathode potential, $\mathrm{V_C}$ at the GDL/GASC interface is imposed for the 'GDL+CL' subdomain. In terms of the electrolyte potential, it is modelled within the 'CL+ELEC' subdomain together. The electrolyte potential, $\mathrm{V_l}$ is set as zero (versus standard hydrogen electrode)[3,45–47] and zero-flux is applied at the CL/GDL boundary.

Model-based performance evaluation

In addition to current density and selectivity, the product yield (PY) and the specific electrical energy consumption (SEEC) should also be considered for scale-up analysis, because they are significant factors for the economic costs of an ECO2RR system.[48] Assuming no losses of $\mathrm{HCOO^-}$, the PY is defined as the mass of formate produced per unit time and is given by:

$$\mathrm{PY} = -\frac{\mathrm{a_{sl}} \mathrm{M_{HCOO}} \mathrm{W_E} \int_0^{\mathrm{H_E}} \int_0^{\mathrm{L_{CL}}} \mathrm{i_{Ea}} \mathrm{dxdy}}{2\mathrm{F}} \tag{27}$$

For the SEEC calculation, we only account for the electricity energy consumed by the electrolyser itself, excluding the consumption by the CO_2 capture process, product purification and auxiliary units such as peristaltic pumps. The SEEC is defined as electric energy consumption for producing a unit mass of the formate product, and is calculated by:

$$\mathrm{SEEC} = \frac{2\mathrm{FV_{app}}}{\mathrm{M_{HCOO}FE_{HCOO}}} \tag{28}$$

$\mathrm{V_{app}}$ represents the required cell voltage and detailed calculation can be found in the SI section IV.

Key parameters are summarised in the SI section II. The model is solved by COMSOL Multiphysics 5.4 with the MUMPS general solver.

Model validation

For the purpose of validation, the simulated total current density is converted to the overall superficial (geometrical) current density with respect to the cathode geometrical surface area, $\mathrm{i_C}$ by:[17]

$$\mathrm{i_C} = \frac{\mathrm{a_{sl}} \int_0^{\mathrm{H_E}} \int_0^{\mathrm{L_{CL}}} (\mathrm{i_{Ea}} + \mathrm{i_{Eb}} + \mathrm{i_{Ec}}) \mathrm{dxdy}}{\mathrm{H_E}} \tag{29}$$

The Faraday efficiency (FE) is the important indicator representing the selectivity. The FEs for $\mathrm{HCOO^-}$, CO and $\mathrm{H_2}$ are defined as:

$$\mathrm{FE_{HCOO}} = \frac{\mathrm{a_{sl}} \int_0^{\mathrm{H_E}} \int_0^{\mathrm{L_{CL}}} \mathrm{i_{Ea}} \mathrm{dxdy}}{\mathrm{i_C H_E}} \times 100\% \tag{30}$$

$$\mathrm{FE_{CO}} = \frac{\mathrm{a_{sl}} \int_0^{\mathrm{H_E}} \int_0^{\mathrm{L_{CL}}} \mathrm{i_{Eb}} \mathrm{dxdy}}{\mathrm{i_C H_E}} \times 100\% \tag{31}$$

$$FE_{H_2} = \frac{a_{sl}\int_0^{H_E}\int_0^{L_{CL}} i_{Ec}\,dxdy}{i_C H_E} \times 100\% \quad (32)$$

The experimental data and the detailed experiment setup can be found in the reference.[4] As indicated by Figure 2, the effects of electrolyte concentration and cathode potential on the i_C and selectivity are predicted by our model with good fidelity at lower KOH concentrations (i.e. 0.5M). However, there is considerable departure between predicted values and experimental data at higher KOH concentrations (i.e. >1.0M), which could be attributed to: (i) C_2 products (i.e. ethyl alcohol and ethylene) are notably generated at higher KOH concentration;[4] (ii) the random error of total current density in experimental measurements enlarges with the KOH concentration higher than 0.5M;[4] (iii) our steady-state model does not reflect the dynamic changes, such as the variation of catalyst size, composition and saturation condition and the effects of these factors tend to be more pronounced with a higher current density (which increases with KOH concentration).[4] Nevertheless, our model is adequate to be used as a predictive tool at least for relatively low KOH concentrations (i.e. $\leq 1.0M$), which have been the main choice of existing GDE experiments.[49–51] Besides, an additional validation of the model based on a GDE experiment with $KHCO_3$ as electrolyte[4] has been conducted which further supports the general validity of the model (see SI section V). In the simulation studies presented below, the system with KOH as the electrolyte has been adopted since it would lead to higher current density and formate yield compared to a system using $KHCO_3$ at the same concentration.[4,12]

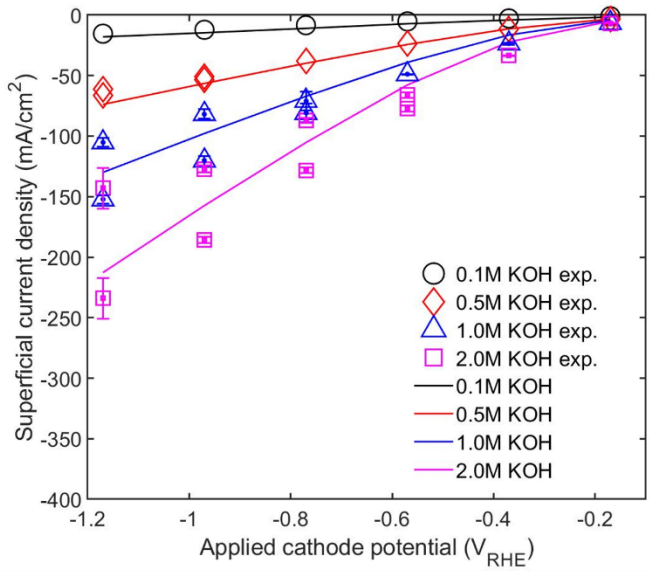

(a)

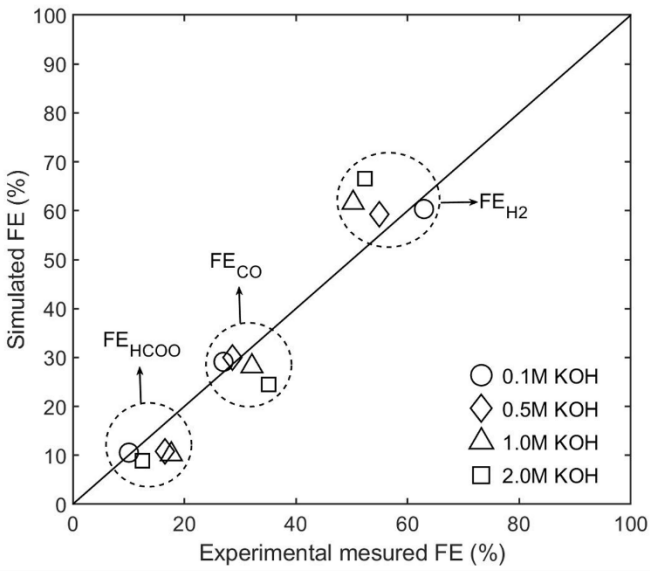

(b)

Figure 2 (a) Overall superficial current density with respect to the cathode geometrical surface area. The lower bound of experimental data of 0.5M, 1.0M and 2.0M KOH are the measured overall superficial current density; the upper bound experimental data are the current density produced by the reaction (Ea) to (Ec) only; (b) Averaged selectivity from data for different cathode potential levels, with various KOH concentrations, compared with calibrated experimental data (excluding products other than H_2, CO and $HCOO^-$).

Results and discussion

Simulation results with various design and operational parameters are presented and interpreted in this section. In comparison with other KOH concentrations, the system with $0.5M\ KOH$ catholyte and at the volumetric flowrate of $0.5\ ml/min$ is selected as it could generate a higher current density and more formate under the same applied cathode potential, without contamination of C2 products. Unless stated otherwise, all other parameters remain as default (see SI Table S12) when the parametric study of a specific factor is carried out, and the description of current density change is in terms of its absolute value.

The effect of the applied cathode potential, V_C

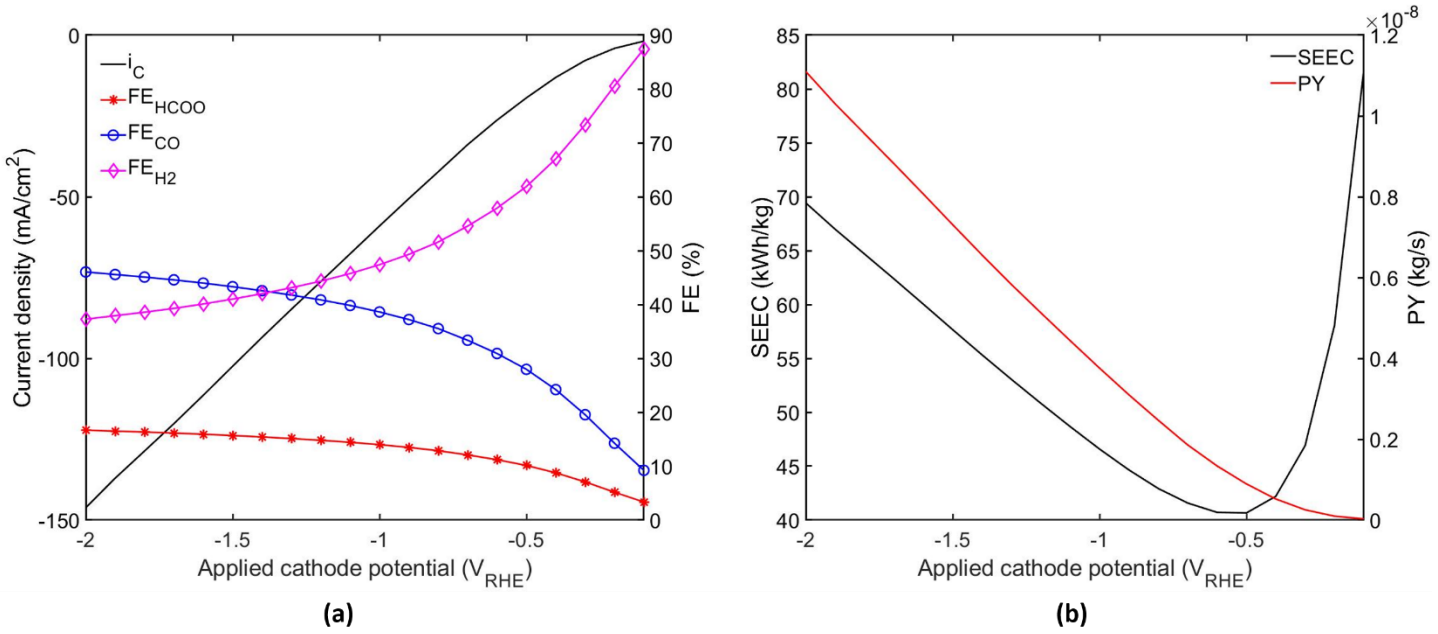

Figure 3 The effect of the applied cathode potential, V_C on (a) overall superficial current density and selectivity; (b) PY and SEEC.

As shown in Figure 3(a), applied cathode potential, $\mathrm{V_C}$ affects the cathodic overall superficial current density, $\mathrm{i_C}$ and selectivity. As $\mathrm{V_C}$ increases, the increases of $\mathrm{i_C}$ (shown in Figure 3(a)) and partial current density for $\mathrm{HCOO^-}$, CO and $\mathrm{H_2}$ (not directly shown in Figure 3(a)) are expected (see Eqs. (19)-(21) and (29)). Owing to a smaller charge transfer coefficient and a significantly lower exchange current density of HER, $\mathrm{FE_{H_2}}$ continuously decreases with more negative $\mathrm{V_C}$, which is desirable; however, $\mathrm{FE_{CO}}$ increases faster than $\mathrm{FE_{HCOO}}$ mainly because less negative $\mathrm{V_C}$ is needed for accelerating $\mathrm{CO_2}$ conversion to CO than to $\mathrm{HCOO^-}$ (i.e. $\mathrm{V_{eq,Eb}}$ is more positive than $\mathrm{V_{eq,Ea}}$). Figure 3(b) shows that PY is improved as $\mathrm{V_C}$ becomes more negative, which is because of the increase in the partial current density for $\mathrm{HCOO^-}$. On SEEC, an optimal value of $\mathrm{V_C}$ of $-0.5\mathrm{V_{RHE}}$ exists; more negative $\mathrm{V_C}$ beyond this point would lead to an increase in PY that cannot compensate the increase in the electrical energy consumption (resulting from the increases in both cell voltage and current). The value of $-0.5\mathrm{V_{RHE}}$ is selected for other parametric studies use (unless specially mentioned).

The GDE scalability

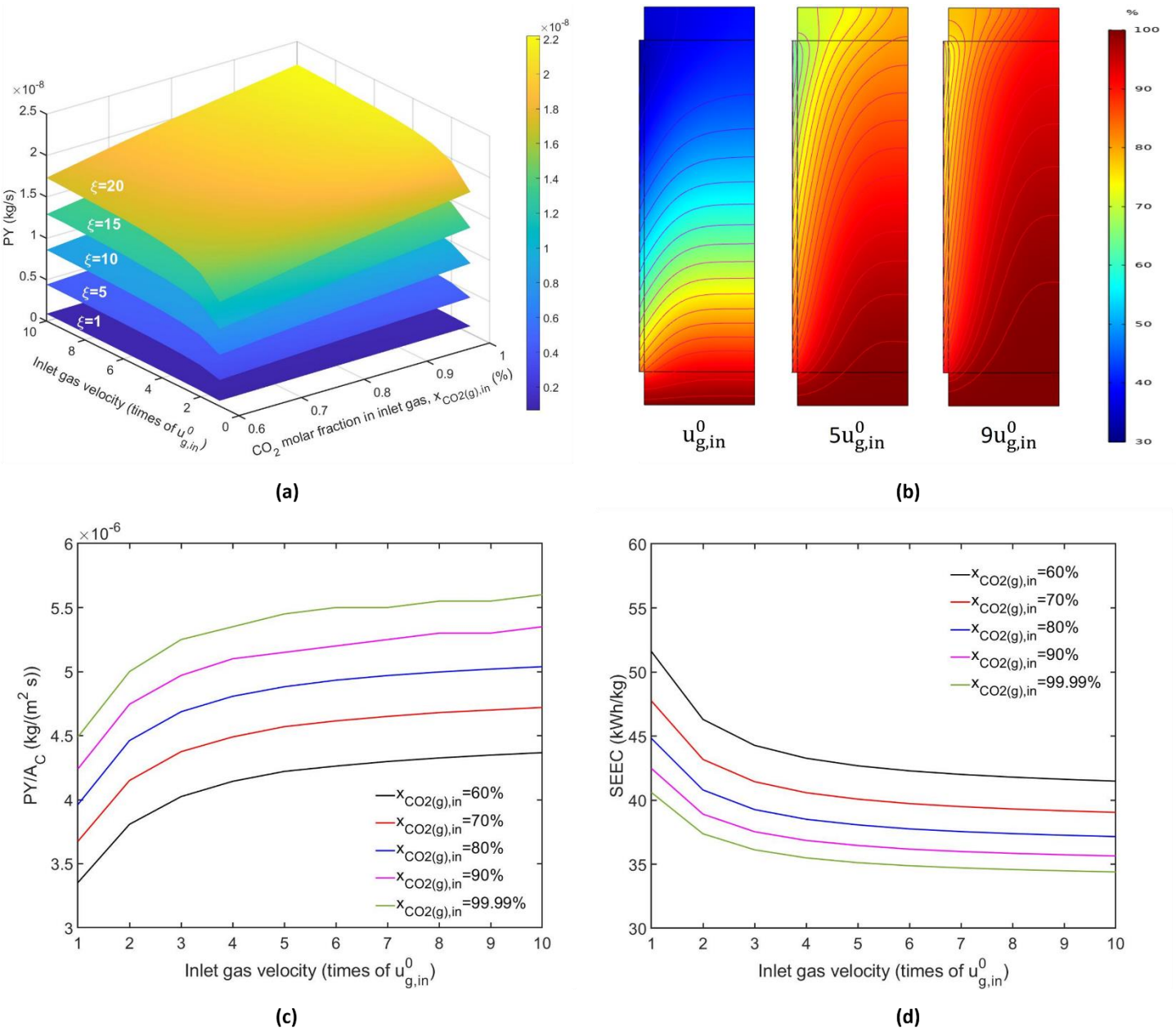

Figure 4 (a) PY with various inlet gas composition and velocity; (b) The distribution of CO_2 molar fraction, $x_{CO_2(g)}$ in the 'GASC+GDL+CL' subdomain with inlet gas velocity; (c) PY/A_C and (d) SEEC for the default system (i.e. ξ=1), as the function of inlet gas velocity and composition.

Larger GDEs can to provide more reaction sites and therefore improve the product yield. To predict the performance of larger-sized GDEs, the cathode geometrical surface area, A_C is upscaled by increasing electrode height, H_E and width, W_E, while keeping the original aspect ratio (i.e. H_E/ W_E). Note that when the thickness of

each compartment remains unchanged, the volume of system scales together with A_C. The upscaling factor, ξ is defined as:

$$\xi = \frac{\text{Upscaled } A_C}{\text{Default } A_C} \tag{33}$$

Two key indicators, PY and SEEC, are still employed to evaluate the performance of the upscaled system. The simulation results suggest that the GDE system is scalable for all the tested conditions (i.e. full tested range of gas velocity and molar fraction of CO_2 in feed gas): (i) the PY is approximately scaled by the same factor of ξ (shown in Figure 4(a) for illustration); (ii) the SEEC is comparable between the larger and smaller electrolysers (observed from simulation results, not shown here); (iii) the selectivity for each testing cases remains almost unchanged (observed from simulation results, not shown here). The first two observations are in accordance with the recently reported experiment finding.[14]

The effect of inlet gas composition and velocity

The impact of the inlet gas velocity, $u_{g,in}$ and the molar fraction of $CO_2(g)$ in feed gas, $x_{CO_2(g),in}$, as two operational settings easy to manipulate, has been discussed in several experimental studies[9,12] and will be examined in this section from the perspective of modelling. For testing, the $u_{g,in}$ is increased up to 10 times of the default value shown in SI Table S4, denoted here by $u_{g,in}^0$ and $x_{CO_2(g),in}$ ranges from 60% to 99.99%. Overall, as shown in Figure 4(a), increasing $CO_2(g)$ supply, including higher $u_{g,in}$ and $x_{CO_2(g),in}$, is helpful to improve PY for different sizes of the GDE. The PY per A_C, PY/A_C and SEEC with various values of $u_{g,in}$ and $x_{CO_2(g),in}$ for the default size of GDE (i.e. $\xi = 1$) are further plotted in Figure 4(c) and (d). One can see that higher $x_{CO_2(g),in}$ always improve both PY/A_C and SEEC. As $u_{g,in}^0$ increases to $5u_{g,in}^0$, both PY/A_C and the SEEC as well as the FE_{HCOO} (not shown) improve remarkably. However, this effect weakens as $u_{g,in}$ increases further. This is due to the trade-

off between $x_{CO_2(g)}$ and total pressure in the CL: a larger $u_{g,in}$ elevates the $x_{CO_2(g)}$ (shown in Figure 4(b)) but at the same time leads to a reduced total pressure in the CL (see SI figure S5(a)); the combined effect is gradually reduced increments of $CO_2(g)$ partial pressure and hence of the gas-liquid mass transfer rate for $CO_2(g)$ (see SI figure S5(b)), eventually causing diminishing improvements to the production of formate. The effects of $u_{g,in}$ and $x_{CO_2(g),in}$ for other larger systems are similar.

The effect of catalyst loading and arrangement

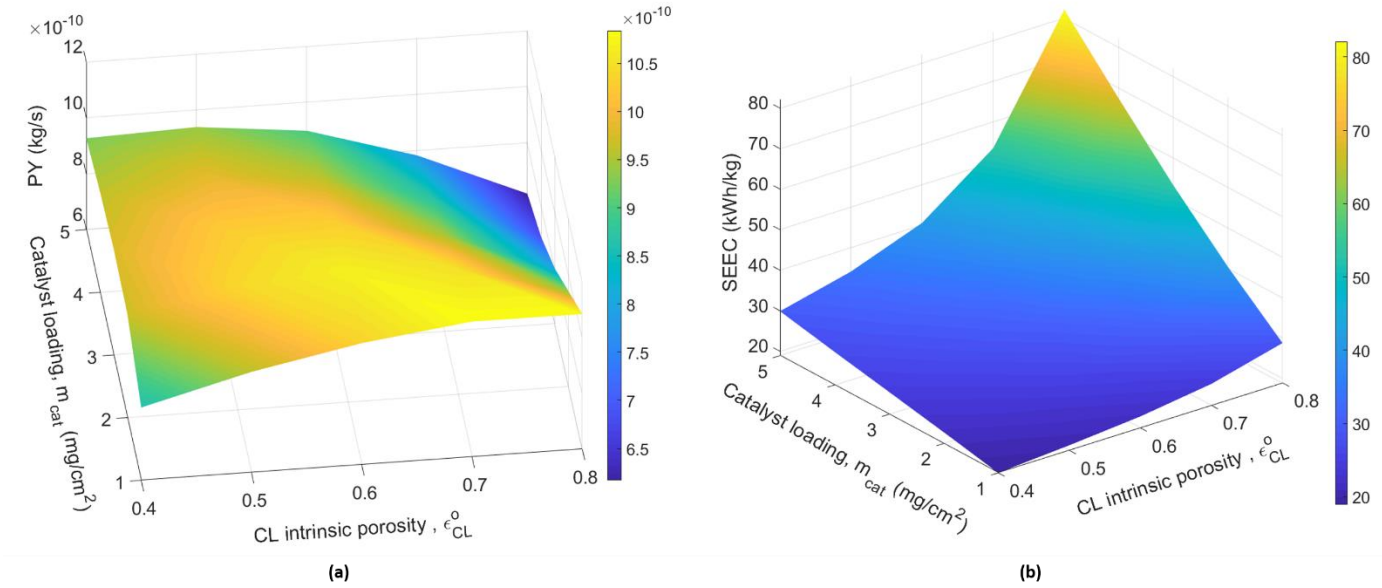

Figure 5 (a) PY and (b) SEEC with different catalyst amount and arrangement.

The catalyst amount and its arrangement can potentially affect both the performance and the cost of the ECO2RR system. In this section, the catalyst loading, m_{cat}, and the catalyst arrangement represented by the intrinsic porosity in the CL, ϵ_{CL}^{o} are discussed. Given the CL manufacture process,[4] the parametric study for the intrinsic porosity in the CL, ϵ_{CL}^{o} is conducted from 0.4 to 0.8, which is in line with the porosity range of random packing arrangements of spherical grains.[52]

Figure 5(a) shows that the effect of m_{cat} on PY varies for different values of ϵ_{CL}^{o}, which reflects the trade-off between multiple factors including particularly CO_2 supply and the provision of the active surface area for

reactions. Based on Eq. (7), L_{CL} would increase with m_{cat} when ϵ_{CL}^{o} is kept constant. On the one hand, for a larger L_{CL} results in a longer path for gas diffusion (along with a greater ohmic loss of potential) which would lead to a lower $CO_2(g)$ partial pressure in the CL (see SI figure S6) and consequently a negative impact on formate generation. On the other hand, an increase of m_{cat} provides a larger active surface for reactions, which potentially improves product generation (see Eq. (27)). For the CL with tighter packing (i.e. $\epsilon_{CL}^{o} < 0.6$), the trade-off of the above factors leads to the occurrence of optimal values of m_{cat} corresponding to the maximum PY (i.e. $3 mg/cm^2$ for the CL with $\epsilon_{CL}^{o} = 0.4$ and $2 mg/cm^2$ for the CL with $0.4 < \epsilon_{CL}^{o} < 0.6$). However, for the looser packing of the CL (i.e. $\epsilon_{CL}^{o} > 0.6$), the losses associated with the increase thickness of the CL and outweighs the gains by the increase in the active surface area, therefore PY continuously drops with the increase in catalyst loading.

Analogous to the preceding analysis, the effect of ϵ_{CL}^{o} on PY is also a result of trade-offs. At a given m_{cat}, the change in ϵ_{CL}^{o} leads to a variation in L_{CL} which impacts on CO_2 supply as discussed above. Additionally, the effective diffusivity $D_{CO_2(g),CL}^{eff}$ (see Eqs. (5) and (6)) and active surface area for gas-liquid mass transfer, a_{gl} (see Eq. (18)) augment with the increase in ϵ_{CL}^{o}, which are instrumental to CO_2 supply and subsequently to the PY. Furthermore, the larger active surface area for electrochemical reactions, a_{sl} (see Eq. (26)) means more sites available for CO_2 reduction process and can potentially increase PY (see Eq. (27)). Besides, ϵ_{CL}^{o} also affects conductivities: the reduced $\sigma_{s,CL}^{eff}$ owing to larger ϵ_{CL}^{o} would lead to a larger voltage drop, although this influence is negligible due to the relatively high value of $\sigma_{s,CL}^{eff}$ in our case (confirmed by the simulation results, not shown here). The $\sigma_{l,CL}^{eff}$ on the other hand increases with a larger ϵ_{CL}^{o}, but the electrolyte potential still drops significantly with the increased L_{CL} and therefore could lead to more positive value of '$V_s - V_l$' (observed from simulation results, not shown here), which is detrimental to CO_2 reduction. With the combined effect of all the

factors, the optimal ϵ_{CL}^{o} that leads to the maximum PY shifts from a higher value to a lower value as m_{cat} increases.

To summarise, the effect of m_{cat} and ϵ_{CL}^{o} on PY is shaped by multiple factors which, in combination, impact on the local value of i_{Ea} and the overall surface area or volume of the CL. Overall, as shown in Figure 5(a), the distribution of $1 mg/cm^2$ catalyst with the intrinsic porosity of 0.7 for the CL, i.e. a design with a low catalyst loading within a "spacious" arrangement, is capable to gain the highest PY (i.e. 1.08×10^{-9} kg/s) within the tested range of settings.

Different from the PY, Figure 5(b) shows that the SEEC always increases with ϵ_{CL}^{o} and m_{cat}, suggesting a more "compact" CL is preferable. The least favourable design in terms of the SEEC (featuring largest ϵ_{CL}^{o} and m_{cat}) coincides with that in terms of the PY, but the optimal setting for the SEEC (featuring lowest ϵ_{CL}^{o} and m_{cat}) corresponds to that leading to an intermediate PY. This is a result of the compromise between the PY and the total energy consumption; the latter is dictated by the larger overpotentials at higher overall currents.

Conclusion

In this paper, gas diffusion electrode (GDE)-based electrochemical conversion of CO_2 to formate together with the by-products (i.e. CO and H_2) was modelled. The two-dimensional steady-state multiphase model was developed by incorporating electrochemical kinetics, the kinetics of homogeneous (aqueous-phase) reactions and transport phenomena in the cathode compartment. This model demonstrated a good agreement with experimental data of current density and selectivity for the system with lower concentrations of KOH and was employed to investigate the effect of applied cathode potential, inlet gas composition and velocity as well as catalyst loading and arrangement on product yield (PY) and specific electrical energy consumption (SEEC).

The simulation results have shown that a more negative cathodic potential results in a higher PY, while the lowest SEEC is reached at an optimal level of $-0.5\mathrm{V_{RHE}}$ with the default settings. The GDE was predicted to be scalable in terms of its cathode geometrical surface area, with respect to selectivity, PY and SEEC. On the impact of design and operational parameters, we have shown that both the PY and the SEEC can be improved by better $\mathrm{CO_2}$ supply through a higher $\mathrm{CO_2}$ feed concentration or a greater gas flowrate, although the improvement by the latter becomes insignificant beyond a certain level as the impact of reduced total pressure amplifies. The PY was shown to be shaped by multiple factors when catalyst loading and arrangement are changed. Resulting from the trade-offs between mass transfer resistance, ohmic loss and effective areas available for mass transfer and reactions, dispersion of $1\mathrm{mg/cm^2}$ catalysts with the porosity of 0.7 in the CL, representing a low loading with a sparse arrangement of catalyst particles, was predicted to be optimal to gain the maximum PY in our study. For the SEEC, its value always becomes larger with $\mathrm{m_{cat}}$ and $\epsilon_{\mathrm{CL}}^{\mathrm{o}}$ resulting from the compromise between the increase in the PY and the increase in overpotential losses, suggesting that higher energy efficiencies may prefer a more compact (i.e. thin and dense) catalyst layer.

Overall, our work demonstrates that a GDE-based device for converting $\mathrm{CO_2}$ with formate as a desirable product has good potential for upscaling, and its performance can be significantly improved by choosing the optimal design and operating settings. These learnings may be applicable to other GDE-based ECO2RR applications. In the future, more efforts could be made to develop a dynamic model to capture further details and integrate with techno-economic analysis and life cycle analysis to gain a holistic understanding of such systems.

Supporting information

Source terms in the CL; key parameter values; specific electrical energy consumption (SEEC); model validation; testing parameter data; profiles of pressure, molar fraction and gas-liquid mass transfer rate.

Conflicts of interest

There are no conflicts to declare.

Acknowledgements

Ziming Yang thanks the China Scholarship Council (CSC) to support her PhD study. The work is supported by the EPSRC LifesCO2R project (EP/N009746/1), the EPSRC NECEM (EP EP/R021503/1), the NERC MeteoRR (NE/L014246/1) and the Open Fund Project of State Key Laboratory of Clean Energy Utilization Project No: ZJUCEU2019004.

Nomenclature

Symbol	Definition
H_{CO_2}	Henry's constant for CO_2, $Pa\ M^{-1}$
K_{GL}	Overall mass transfer coefficient, $m\ s^{-1}$
R_{ideal}	Ideal gas constant, $J\ mol^{-1}\ K^{-1}$
a	Specific interfacial area, m^{-1}
A	Area, m^2
C	Concentration, M
d	Diameter, m
D	Molecular diffusivity, $m^2\ s^{-1}$
F	Faraday constant, $s\ A\ mol^{-1}$
FE	Faraday efficiency, %
g	Gravitational acceleration, $m\ s^{-2}$
H	Height (y-axis), m
i	Current density, $A\ m^{-2}$
k	Reaction rate constant, $M^{-1}s^{-1}$
K	Equilibrium constant, M^{-1}
L	Thickness (x-axis) or distance, m

m	Mass loading, $kg\ m^{-2}$
M	Molar weight, $kg\ mol^{-1}$
n	Number of transferred electrons, dimensionless
P	Pressure, Pa
PY	Product (i.e. formate) yield, $kg\ s^{-1}$
Q	Source term, its unit relying on the specific reactions
q	Volumetric flowrate, $m^3\ s^{-1}$
R	Volumetric reaction rate on the mass basis, $kg\ m^{-3}\ s^{-1}$
r	Radius, m
S	Saturation coefficient, dimensionless
$SEEC$	Specific electrical energy consumption, $kWh\ kg\ (formate)^{-1}$
T	Operating temperature, K
u	Velocity, $m\ s^{-1}$
V	Potential, V
W	Width, m
x	Molar fraction, dimensionless
z	Valence of ionic species
β	Symmetry factor, dimensionless
δ	Thickness, m
ϵ	Porosity, dimensionless
κ	Permeability, m^2
μ	Dynamic viscosity, $Pa\ s$
ξ	Scale-up factor, dimensionless
ρ	Density, $kg\ m^{-3}$
σ	Conductivity, $S\ m^{-1}$
ω	Mass fraction, dimensionless
Subscript	
app	Applied/required external potential
aq	Dissolved species
b	Bulk phase

C	Cathode
cat	Catalyst
CL	Catalyst layer
d	Diffusion
E	Electrode
Ea	Electrochemical reaction, Ea
Eb	Electrochemical reaction, Eb
Ec	Electrochemical reaction, Ec
ele	Electrolyte
ELEC	Electrolyte channel
eq	Equilibrium
EXT	Extension
g	Mixture gas
GASC	Gas chamber
GDL	Gas diffusion layer
H	Homogeneous reactions
Ha	Homogeneous reaction, Ha
Hb	Homogeneous reaction, Hb
i	Gaseous species
in	Inlet gas
j	Aqueous species
k	Gaseous species, $k \neq i$
m	Medium
o	Exchange current density
P	Gas-liquid mass transfer
p	Porous
RHE	Reversible hydrogen electrode
s	Electronic (solid material) potential
Superscript	
0	Intrinsic characteristics

eff	Effective characteristics
o	Theoretical value
ref	Reference condition

Abbreviation	
CCU	Carbon capture and utilisation
CL	Catalyst layer
ECO2RR	Electrochemical CO_2 reduction reaction
ELEC	Electrolyte channel
FE	Faraday efficiency
GASC	Gas chamber
GDE	Gas diffusion electrode
GDL	Gas diffusion layer
HER	Hydrogen evolution reaction
LHS	Left-hand side (of an equation)
MEAs	Membrane-electrode-assemblies
PY	Product yield
RDS	Rate-determining step
SEEC	Specific electrical energy consumption

References

(1) Nguyen, T. N.; Dinh, C.-T. Gas Diffusion Electrode Design for Electrochemical Carbon Dioxide Reduction. *Chem. Soc. Rev.* **2020**, *49* (21), 7488–7504, DOI 10.1039/d0cs00230e.

(2) García de Arquer, F. P.; Dinh, C. T.; Ozden, A.; Wicks, J.; McCallum, C.; Kirmani, A. R.; Nam, D. H.; Gabardo, C.; Seifitokaldani, A.; Wang, X.; Li, Y. C.; Li, F.; Edwards, J.; Richter, L. J.; Thorpe, S. J.; Sinton, D.; Sargent, E. H. CO2 Electrolysis to Multicarbon Products at Activities Greater than 1 A Cm−2. *Science.* **2020**, *367*, 661–666, DOI 10.1126/science.aay4217.

(3) Weng, L. C.; Bell, A. T.; Weber, A. Z. Modeling Gas-Diffusion Electrodes for CO2 Reduction. *Phys. Chem.*

Chem. Phys. **2018**, *20*, 16973–16984, DOI 10.1039/c8cp01319e.

(4) Xiang, H.; Rasul, S.; Scott, K.; Portoles, J.; Cumpson, P.; Yu, E. H. Enhanced Selectivity of Carbonaceous Products from Electrochemical Reduction of CO2 in Aqueous Media. *J. CO2 Util.* **2019**, *30*, 214–221, DOI 10.1016/j.jcou.2019.02.007.

(5) Lu, X.; Leung, D. Y. C.; Wang, H.; Leung, M. K. H.; Xuan, J. Electrochemical Reduction of Carbon Dioxide to Formic Acid. *ChemElectroChem* **2014**, *1*, 836–849, DOI 10.1002/celc.201300206.

(6) Newman, J.; Tiedemann, W. Porous-electrode Theory with Battery Applications. *AIChE J.* **1975**, *21* (1), 25–41, DOI 10.1002/aic.690210103.

(7) Liang, S.; Altaf, N.; Huang, L.; Gao, Y.; Wang, Q. Electrolytic Cell Design for Electrochemical CO2 Reduction. *J. CO2 Util.* **2020**, *35*, 90–105, DOI 10.1016/j.jcou.2019.09.007.

(8) De Mot, B.; Hereijgers, J.; Duarte, M.; Breugelmans, T. Influence of Flow and Pressure Distribution inside a Gas Diffusion Electrode on the Performance of a Flow-by CO2 Electrolyzer. *Chem. Eng. J.* **2019**, *378*, 122224, DOI 10.1016/j.cej.2019.122224.

(9) Tan, Y. C.; Lee, K. B.; Song, H.; Oh, J. Modulating Local CO2 Concentration as a General Strategy for Enhancing C−C Coupling in CO2 Electroreduction. *Joule* **2020**, *4*, 1104–1120, DOI 10.1016/j.joule.2020.03.013.

(10) Whipple, D. T.; Kenis, P. J. A. Prospects of CO2 Utilization via Direct Heterogeneous Electrochemical Reduction. *J. Phys. Chem. Lett.* **2010**, *1*, 3451–3458, DOI 10.1021/jz1012627.

(11) Lee, M. Y.; Park, K. T.; Lee, W.; Lim, H.; Kwon, Y.; Kang, S. Current Achievements and the Future Direction of Electrochemical CO2 Reduction: A Short Review. *Crit. Rev. Environ. Sci. Technol.* **2020**, *50* (8), 769–815, DOI 10.1080/10643389.2019.1631991.

(12) Gabardo, C. M.; O'Brien, C. P.; Edwards, J. P.; McCallum, C.; Xu, Y.; Dinh, C. T.; Li, J.; Sargent, E. H.;

Sinton, D. Continuous Carbon Dioxide Electroreduction to Concentrated Multi-Carbon Products Using a Membrane Electrode Assembly. *Joule* **2019**, *3*, 2777–2791, DOI 10.1016/j.joule.2019.07.021.

(13) Li, H.; Oloman, C. Development of a Continuous Reactor for the Electro-Reduction of Carbon Dioxide to Formate - Part 2: Scale-Up. *J. Appl. Electrochem.* **2007**, *37*, 1107–1117, DOI 10.1007/s10800-007-9371-8.

(14) Jeanty, P.; Scherer, C.; Magori, E.; Wiesner-Fleischer, K.; Hinrichsen, O.; Fleischer, M. Upscaling and Continuous Operation of Electrochemical CO2 to CO Conversion in Aqueous Solutions on Silver Gas Diffusion Electrodes. *J. CO2 Util.* **2018**, *24*, 454–462, DOI 10.1016/j.jcou.2018.01.011.

(15) Krause, R.; Reinisch, D.; Reller, C.; Eckert, H.; Hartmann, D.; Taroata, D.; Wiesner-Fleischer, K.; Bulan, A.; Lueken, A.; Schmid, G. Industrial Application Aspects of the Electrochemical Reduction of CO2 to CO in Aqueous Electrolyte. *Chemie-Ingenieur-Technik* **2020**, *92*, 53–61, DOI 10.1002/cite.201900092.

(16) Wang, H.; Leung, D. Y. C.; Xuan, J. Modeling of a Microfluidic Electrochemical Cell for CO2 Utilization and Fuel Production. *Appl. Energy* **2013**, *102*, 1057–1062, DOI 10.1016/j.apenergy.2012.06.020.

(17) Wu, K.; Birgersson, E.; Kim, B.; Kenis, P. J. A.; Karimi, I. A. Modeling and Experimental Validation of Electrochemical Reduction of CO2 to CO in a Microfluidic Cell. *J. Electrochem. Soc.* **2015**, *162* (1), F23–F32, DOI 10.1149/2.1021414jes.

(18) Georgopoulou, C.; Jain, S.; Agarwal, A.; Rode, E.; Dimopoulos, G.; Sridhar, N.; Kakalis, N. On the Modelling of Multidisciplinary Electrochemical Systems with Application on the Electrochemical Conversion of CO2 to Formate/Formic Acid. *Comput. Chem. Eng.* **2016**, *93*, 160–170, DOI 10.1016/j.compchemeng.2016.06.012.

(19) Weng, L. C.; Bell, A. T.; Weber, A. Z. Towards Membrane-Electrode Assembly Systems for CO2 Reduction: A Modeling Study. *Energy Environ. Sci.* **2019**, *12*, 1950–1968, DOI 10.1039/c9ee00909d.

(20) Weng, L.-C.; Bell, A. T.; Weber, A. Z. A Systematic Analysis of Cu-Based Membrane-Electrode Assemblies for CO2 Reduction through Multiphysics Simulation. *Energy Environ. Sci.* **2020**, *13*, 3592–3606, DOI 10.1039/d0ee01604g.

(21) Garg, S.; Li, M.; Weber, A. Z.; Ge, L.; Li, L.; Rudolph, V.; Wang, G.; Rufford, T. E. Advances and Challenges in Electrochemical CO2 Reduction Processes: An Engineering and Design Perspective Looking beyond New Catalyst Materials. *J. Mater. Chem. A* **2020**, *8*, 1511–1544, DOI 10.1039/c9ta13298h.

(22) Zhong, H.; Fujii, K.; Nakano, Y.; Jin, F. Effect of CO2 Bubbling into Aqueous Solutions Used for Electrochemical Reduction of CO2 for Energy Conversion and Storage. *J. Phys. Chem. C* **2015**, *119*, 55–61, DOI 10.1021/jp509043h.

(23) Hori, Y.; Murata, A.; Takahashi, R. Formation of Hydrocarbons in the Electrochemical Reduction of Carbon Dioxide at a Copper Electrode in Aqueous Solution. *J. Chem. Soc. Faraday Trans. 1 Phys. Chem. Condens. Phases* **1989**, *85* (8), 2309–2326, DOI 10.1039/f19898502309.

(24) Hori, Y.; Suzuki, S. Electrolytic Reduction of Bicarbonate Ion at a Mercury Electrode. *J. Electrochem. Soc.* **1983**, *130*, 2387, DOI 10.1149/1.2119593.

(25) Kumar, B.; Llorente, M.; Froehlich, J.; Dang, T.; Sathrum, A.; Kubiak, C. P. Photochemical and Photoelectrochemical Reduction of CO2. *Annu. Rev. Phys. Chem.* **2012**, *63*, 541–569, DOI 10.1146/annurev-physchem-032511-143759.

(26) Haas, T.; Krause, R.; Weber, R.; Demler, M.; Schmid, G. Technical Photosynthesis Involving CO2 Electrolysis and Fermentation. *Nat. Catal.* **2018**, *1*, 32–39, DOI 10.1038/s41929-017-0005-1.

(27) Ma, S.; Sadakiyo, M.; Luo, R.; Heima, M.; Yamauchi, M.; Kenis, P. J. A. One-Step Electrosynthesis of Ethylene and Ethanol from CO2 in an Alkaline Electrolyzer. *J. Power Sources* **2016**, *301*, 219–228, DOI 10.1016/j.jpowsour.2015.09.124.

(28) Qiao, J.; Fan, M.; Fu, Y.; Bai, Z.; Ma, C.; Liu, Y.; Zhou, X. D. Highly-Active Copper Oxide/Copper Electrocatalysts Induced from Hierarchical Copper Oxide Nanospheres for Carbon Dioxide Reduction Reaction. *Electrochim. Acta* **2015**, *153*, 559–565, DOI 10.1016/j.electacta.2014.09.147.

(29) Kotb, Y.; Fateen, S. E. K.; Albo, J.; Ismail, I. Modeling of a Microfluidic Electrochemical Cell for the Electro-Reduction of CO2 to CH3OH. *J. Electrochem. Soc.* **2017**, *164* (13), E391–E400, DOI 10.1149/2.0741713jes.

(30) J.Kee, R.; Coltrin, M. E.; Glarborg, P.; Zhu, H. *Chemically Reacting Flow*; 2003.

(31) Torstensson, M. A Comparison of the Multicomponent Model and the Mixture Averaged Approximation, 2014.

(32) Bongers, H.; De Goey, L. P. H. The Effect of Simplified Transport Modeling on the Burning Velocity of Laminar Premixed Flames. *Combust. Sci. Technol.* **2003**, *175*, 1915–1928, DOI 10.1080/713713111.

(33) Balliet, R. J.; Newman, J. Cold Start of a Polymer-Electrolyte Fuel Cell I. Development of a Two-Dimensional Model. *J. Electrochem. Soc.* **2011**, *158* (8), B927–B938, DOI 10.1149/1.3592430.

(34) Serincan, M. F.; Pasaogullari, U.; Sammes, N. M. Effects of Operating Conditions on the Performance of a Micro-Tubular Solid Oxide Fuel Cell (SOFC). *J. Power Sources* **2009**, *192*, 414–422, DOI 10.1016/j.jpowsour.2009.03.049.

(35) Bear, J. *Dynamics of Fluids in Porous Media*; Amerian Elsevier publishing company, 1972.

(36) M. Kaviany. *Principles of Heat Transfer in Porous Media*, Second edi.; Springer: New York, 1999.

(37) Nam, J. H.; Kaviany, M. Effective Diffusivity and Water-Saturation Distribution in Single- and Two-Layer PEMFC Diffusion Medium. *Int. J. Heat Mass Transf.* **2003**, *46*, 4595–4611, DOI 10.1016/S0017-9310(03)00305-3.

(38) Weber, A. Z.; Newman, J. Modeling Transport in Polymer-Electrolyte Fuel Cells. *Chem. Rev.* **2004**, *104*

(10), 4679–4726, DOI 10.1021/cr020729l.

(39) Zhang, B.; Ye, D. D.; Sui, P. C.; Djilali, N.; Zhu, X. Computational Modeling of Air-Breathing Microfluidic Fuel Cells with Flow-over and Flow-through Anodes. *J. Power Sources* **2014**, *259*, 15–24, DOI 10.1016/j.jpowsour.2014.02.076.

(40) Mo, Z.; Friedly, J. C. Local Reaction and Diffusion in Porous Media Transport Models. *Water Resour. research* **2000**, *36* (2), 431–438, DOI 10.1029/1999WR900308.

(41) Cheng, T.; Xiao, H.; Goddard, W. A. Reaction Mechanisms for the Electrochemical Reduction of CO2 to CO and Formate on the Cu(100) Surface at 298 K from Quantum Mechanics Free Energy Calculations with Explicit Water. *J. Am. Chem. Soc.* **2016**, *138*, 13802–13805, DOI 10.1021/jacs.6b08534.

(42) Wei, J.; Zhou, M.; Long, A.; Xue, Y.; Liao, H.; Wei, C.; Xu, Z. J. Heterostructured Electrocatalysts for Hydrogen Evolution Reaction under Alkaline Conditions. *Nano-Micro Lett.* **2018**, 10:75, DOI 10.1007/s40820-018-0229-x.

(43) Bernardi, Dawn M., Verbrugge, M. W. Mathematical Model of a Gas Diffusion Electrode Bonded to a Polymer Electrolyte. *AIChE J.* **1991**, *37* (8), 1151–1163, DOI 10.1002/aic.690370805.

(44) Xing, L.; Mamlouk, M.; Kumar, R.; Scott, K. Numerical Investigation of the Optimal Nafion® Ionomer Content in Cathode Catalyst Layer: An Agglomerate Two-Phase Flow Modelling. *Int. J. Hydrogen Energy* **2014**, *39*, 9087–9104, DOI 10.1016/j.ijhydene.2014.03.225.

(45) Björnbom, P. Influence of Diffusion Resistances on Gas Diffusion Electrodes. *J. Electrochem. Soc.* **1986**, *133* (9), 1874–1875, DOI 10.1149/1.2109039.

(46) Buck, R. P. Kinetics of Bulk and Interfacial Ionic Motion: Microscopic Basis and Limits for the Nernst-Planck Equation Applied to Membrane Systems. *J. Memb. Sci.* **1984**, *17*, 1–62, DOI 10.1016/S0376-7388(00)81386-1.

(47) Baker, D. R. Reducing Nonlinear Systems of Transport Equations to Laplace's Equation. *SIAM J. Appl. Math.* **1993**, *53* (2), 419–439, DOI 10.1137/0153024.

(48) Spurgeon, J. M.; Kumar, B. A Comparative Technoeconomic Analysis of Pathways for Commercial Electrochemical CO2 Reduction to Liquid Products. *Energy Environ. Sci.* **2018**, *11*, 1536–1551, DOI 10.1039/c8ee00097b.

(49) Xiang, H.; Miller, H. A.; Bellini, M.; Christensen, H.; Scott, K.; Rasul, S.; Yu, E. H. Production of Formate by CO2 Electrochemical Reduction and Its Application in Energy Storage. *Sustain. Energy Fuels* **2020**, *4*, 277–284, DOI 10.1039/c9se00625g.

(50) Endrődi, B.; Bencsik, G.; Darvas, F.; Jones, R.; Rajeshwar, K.; Janáky, C. Continuous-Flow Electroreduction of Carbon Dioxide. *Prog. Energy Combust. Sci.* **2017**, *62*, 133–154, DOI 10.1016/j.pecs.2017.05.005.

(51) Xiang, H.; Rasul, S.; Hou, B.; Portoles, J.; Cumpson, P.; Yu, E. H. Copper-Indium Binary Catalyst on a Gas Diffusion Electrode for High-Performance CO2 Electrochemical Reduction with Record CO Production Efficiency. *ACS Appl. Mater. Interfaces* **2020**, *12*, 601–608, DOI 10.1021/acsami.9b16862.

(52) Gueguen, Y.; Victor Palciauskas. *Introduction to the Physics of Rocks*; Princeton university press: Princeton, 1994.

"For Table of Contents Use Only."

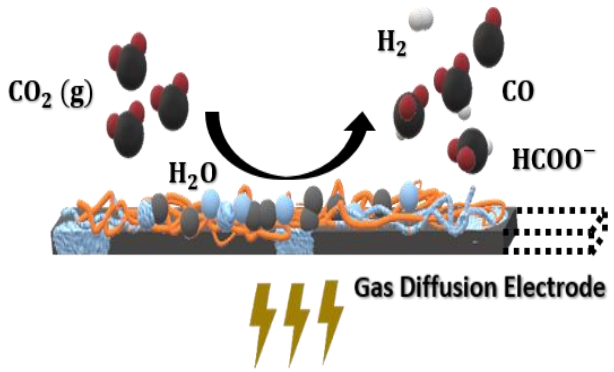

Synopsis

Electrochemical CO_2 reduction systems incorporating gas diffusion electrodes have the potential to transform CO_2 to valuable products efficiently and environment-friendly.